Your thesaurus codes are:
20(08.09.2 HD 93521; 09.12.1; 09.13.2; 13.21.3; 13.21.5)

ASTROPHYSICS
June 23, 2000

The ORFEUS II Echelle Spectrum of HD 93521: A reference for interstellar molecular hydrogen

J. Barnstedt[1], **W. Gringel**[1], **N. Kappelmann**[1], **and M. Grewing**[1,2]

[1] Institut für Astronomie und Astrophysik, Abt. Astronomie, Eberhard-Karls-Universität Tübingen, Waldhäuserstr. 64, D-72076 Tübingen, Germany
[2] Institut de Radio Astronomie Millimétrique (IRAM), 300 Rue de la Piscine, F-38406 Saint Martin d'Hères, France

Received December 13, 1999; accepted January 21, 2000

Abstract. During the second flight of the *ORFEUS-SPAS* mission in November/December 1996, the Echelle spectrometer was used extensively by the Principal and Guest Investigator teams as one of the two focal plane instruments of the *ORFEUS* telescope. The spectrum of HD 93521 was obtained during this mission with a total integration time of 1740 s. This spectrum shows numerous sharp interstellar absorption lines. We identified 198 lines of molecular hydrogen including at least 7 lines with a high velocity component. Also most of the 67 identified interstellar metal lines are visible with a high velocity component.

We present plots of the complete *ORFEUS II* Echelle spectrum together with tables of all identified interstellar absorption lines including all 14 detectable H I lines. In addition several identified stellar lines, partially with narrow absorption components, and stellar wind lines are given in a separate table.

Key words: Stars: individual: HD 93521 – ISM: lines and bands – ISM: molecules – Ultraviolet: ISM – Ultraviolet: stars

1. Introduction

The star HD 93521 is a high galactic latitude O-star. It has been used for many years as a tracer of the interstellar gas in the galactic halo, for which it is well suited due to its brightness ($V = 7.04$), high galactic latitude ($l = 183°$, $b = 62°$) and large rotational velocity ($v \sin i \approx 400\,\mathrm{km\,s^{-1}}$, Lennon et al. 1991). Together with a z-distance of about 1.5 kpc (Irvine 1989), HD 93521 is an ideal candidate for studying kinematics of the halo gas, since galactic rotation effects should be very small (Spitzer & Fitzpatrick 1992).

With the Echelle spectrometer of the *ORFEUS* telescope (Orbiting and Retrievable Far and Extreme Ultraviolet Spectrometer) it was for the first time possible to observe all available absorption lines of interstellar molecular hydrogen towards HD 93521. In the gathered spectra we identified 198 H_2-lines. These lines are very narrow and strong but unsaturated, which was the reason why many of them were used for wavelength calibration of the *ORFEUS* Echelle spectrometer. Also 67 other interstellar absorption lines and 14 lines of the Lyman series were identified. For completeness stellar and stellar wind absorption lines are shown too.

We present the whole Echelle spectrum of HD 93521, obtained during the second *ORFEUS-SPAS* mission in November/December 1996. This spectrum has a good signal to noise ratio and the spectral resolution achieved is somewhat higher than the claimed resolution of $\lambda/\Delta\lambda = 10.000$ (Barnstedt et al. 1999).

The plots presented in the appendix show one Echelle order per plot for wavelengths above 1130 Å (Echelle orders 40 to 49), and half an Echelle order per plot for Echelle orders 50 to 61 ($\lambda < 1130$ Å) where all H_2-lines are included.

2. Data reduction and line identification

Two separate observations of HD 93521 were obtained during two successive orbits with a total integration time of 1740 s (ORFEUS observation IDs 2276_2 and 2276_3, observation date: day 333 of 1996, GMT 04:56:05 – 05:14:05 and GMT 06:28:05 – 06:39:05). The two echelle images were coadded and then the standard extraction procedure was applied (Barnstedt et al. 1999) without any smoothing. An additional radial velocity correction of $-10\,\mathrm{km\,s^{-1}}$ was applied, which corrects the wavelength scale for the fact that the star was not absolutely centered in the entrance diaphragm of the telescope. The maximum uncertainty due to the 20″ diameter of the diaphragm was $\pm 36\,\mathrm{km\,s^{-1}}$, so the deviation of $-10\,\mathrm{km\,s^{-1}}$ corresponds to a pointing offset of 3″, which is an excellent value for the *ASTRO-SPAS* satellite. The value of $-10\,\mathrm{km\,s^{-1}}$ was estimated by comparing the observed radial velocity components with those already published (Spitzer & Fitzpatrick 1992). The wavelength scale is he-

Send offprint requests to: J. Barnstedt
e-mail: barnstedt@astro.uni-tuebingen.de

liocentric, a LSR scale would require an additional correction of $-1.6\,\mathrm{km\,s^{-1}}$, which is negligible.

As with all echelle spectra, the signal to noise ratio is best in the centre of the echelle orders, while it is reduced by a factor of about 1.4 at both ends of each order. Due to the blaze curve being not fully centered, the signal to noise ratio at the short wavelength end is significantly better than at the long wavelength end of each echelle order. There is also a slight deviation in the wavelength calibration at the short wavelength end of each order, which affects a wavelength range of about 5% in each order.

For line identifications we used the following line catalogues:

1. H_2-lines:
   - Morton & Dinerstein (1976), except L10P1
   - Abgrall et al. (1993), correct wavelength for L10P1: 982.834 Å
2. Metal lines and H I:
   - Morton (1991)
   - Kurucz CD No. 23, web-page (Kurucz 1995)
   - Kelly (1968; and web-page)
   - Feibelman & Johannson (1995)

Identified lines from IUE spectra of HD 93521 above 1170 Å are listed by Ramella et al. (1980), with exception of two interstellar lines: λ1260.4, which is Si II and not Si III, and λ1304.4, which is also Si II and not O I.

The tables and plots show blended lines also, for which a non-ambiguous identification or estimate of the intensity is not possible.

Lines with a lower energy level greater than zero are marked with an asterisk, *. All stellar lines are marked with a bracketed asterisk, (*), and stellar wind lines are marked as (w) in the plots as well as in the tables.

3. Discussion of spectral features

The interstellar, stellar and wind absorption lines are visible in several or different radial velocity components. We therefore list and describe all occuring radial velocity components in Table 1.

We present tables of identified interstellar and stellar absorption lines. These tables show a running number for identification of the lines in the plots shown in the appendix, the vacuum wavelength, the $\log(gf)$-value, the number of the radial velocity component (VC) applied as given in Table 1, and some remarks or the transition for the H_2-lines. We will present and discuss the tables of molecular hydrogen lines, other interstellar lines, Lyman series lines and stellar absorption lines.

3.1. Radial velocity components

Table 1 lists 7 components of radial velocities used to identify absorption lines and features in the spectrum. The first two components are the interstellar absorptions at $-12\,\mathrm{km\,s^{-1}}$ and $-60\,\mathrm{km\,s^{-1}}$, which are the two strongest of well known interstellar components (Grewing et al. 1978; Keenan et al. 1995; Spitzer & Fitzpatrick 1992, 1993). No. 3 gives the published value of the radial velocity of HD 93521 of $-16\,\mathrm{km\,s^{-1}}$(*SIMBAD*). No. 4 is the velocity of the emission of the geocoronal Ly-α line. This emission line results from a completely illuminated entrance aperture of the Echelle spectrometer which had a projected diameter of 20″. The velocity of $36.5\,\mathrm{km\,s^{-1}}$ is the negative sum of two wavelength corrections applied to this spectrum: the heliocentric correction and the decentering correction ($26.5\,\mathrm{km\,s^{-1}}$+$10\,\mathrm{km\,s^{-1}}$).

Some stellar absorption lines show narrow absorption components resulting from winds, which have been observed previously (Bjorkman et al. 1994), but which are varying in time. We have identified two such components in serveral lines and they are listed as numbers 5 and 6 in Table 1. Component 7 represents the radial velocities of the strong Si III $\lambda\lambda$1300 triplets, which are also due to stellar wind absorption (Massa 1995).

Table 1. Table of radial velocity components (VC).

VC No.	Rad.vel. [km/s]	Description
1	−12	first (main) interstellar component
2	−60	high velocity interstellar component
3	−16	radial velocity of HD 93521
4	36.5	geocoronal Ly-α emission
5	−270	1. wind feature in stellar absorption lines
6	−340	2. wind feature in stellar absorption lines
7	−80	wind feature in Si III triplets

3.2. Interstellar molecular hydrogen

For most of the H_2-lines only the main velocity component no. 1 was observed, but for some unblended lines the high velocity component could be seen also. A detailed discussion of column densities and curve of growths will be published in a separate paper (Gringel et al., in preparation).

Previous *Copernicus* measurements of selected H_2-lines only led to an upper limit of $\log N(H_2) < 18.54$ (Savage et al. 1992). The high velocity components were not detected by *Copernicus*.

Table 2. Table of identified or possible interstellar molecular hydrogen lines. VC is the velocity component as given in Table 1.

No.	λ [Å]	$\log(f)$	VC	Transition	Remarks
1	918.411	−2.795	1	L18P1	blend
2	918.427	−1.889	1	W5Q3	blend
3	919.410	−2.430	1	L18R2	blend

Table 2, continued ...

No.	λ [Å]	$\log(f)$	VC	Transition	Remarks
4	919.545	−2.345	1	W5P3	blend
5	920.242	−2.767	1	L18P2	
6	924.643	−2.412	1	L17R1	
7	925.173	−2.707	1	L17P1	
8	927.020	−2.628	1	L17P2	
9	928.437	−2.548	1	L17R3	
10	929.534	−1.470	1	W4R0	blend
11	929.687	−1.810	1	W4R1	blend
12	929.688	−2.595	1	L17P3	blend
13	931.063	−1.991	1	L16R0	
14	931.732	−2.151	1	L16R1	blend
15	931.779	−1.714	1	W4Q2	blend
16	931.811	−1.979	1	W4R3	blend
17	932.270	−2.621	1	L16P1	
18	932.606	−2.318	1	W4P2	
19	933.185	−2.563	1	L17P4	blend
20	933.243	−2.202	1	L16R2	blend
21	933.581	−1.714	1	W4Q3	
22	934.146	−2.643	1	L16P2	
23	934.789	−2.145	1	W4P3	
24	935.537	−2.498	1	L17R5	blend
25	935.578	−2.236	1	L16R3	blend
26	935.959	−1.717	1	W4Q4	
27	936.859	−2.679	1	L16P3	
28	938.468	−2.036	1	L15R0	
29	939.124	−2.207	1	L15R1	
30	939.710	−2.536	1	L15P1	
31	940.627	−2.256	1	L15R2	
32	941.601	−2.471	1	L15P2	
33	942.966	−2.293	1	L15R3	
34	944.331	−2.451	1	L15P3	
35	946.129	−2.342	1	L15R4	blend
36	946.170	−2.958	1	L14R0	blend
37	946.386	−1.889	1	W3R1	blend
38	946.425	−1.207	1	W3R0	blend
39	946.986	−2.728	1	L14R1	blend
40	947.113	−1.876	1	W3R2	
41	947.425	−1.564	1	W3Q1	
42	947.517	−2.454	1	L14P1	
43	948.418	−1.893	1	W3R3	blend
44	948.472	−1.917	1	L14R2	blend
45	948.618	−1.564	1	W3Q2	blend
46	949.355	−2.041	1	L14P2	blend
47	950.316	−1.903	1	W3R4	blend
48	950.401	−1.564	1	W3Q3	blend
49	950.820	−2.003	1	L14R3	blend
50	951.672	−1.896	1	W3P3	
51	952.256	−2.416	1	L15P5	blend
52	952.276	−3.151	1	L14P3	blend
53	952.758	−1.565	1	W3Q4	blend
54	952.807	−1.762	1	W3R5	blend
55	954.419	−1.860	1	L13R0	blend
56	954.475	−1.873	1	W3P4	blend
57	955.067	−2.024	1	L13R1	
58	955.682	−1.567	1	W3Q5	
59	955.711	−2.374	1	L13P1	
60	956.581	−2.064	1	L13R2	
61	957.654	−2.316	1	L13P2	

Table 2, continued ...

No.	λ [Å]	$\log(f)$	VC	Transition	Remarks
62	958.949	−2.087	1	L13R3	
63	960.452	−2.307	1	L13P3	
64	962.978	−1.889	1	L12R0	
65	963.609	−2.163	1	L12R1	blend
66	964.312	−2.300	1	L12P1	
67	964.988	−2.821	1	L12R2	blend
68	964.988	−1.162	1	W2R0	blend
69	965.067	−1.453	1	W2R1	blend
70	965.793	−1.491	1	W2R2	
71	966.097	−1.457	1	W2Q1	
72	966.272	−2.189	1	L12P2	
73	966.780	−2.104	1	W2R3	
74	967.278	−1.458	1	W2Q2	
75	967.674	−1.667	1	L12R3	
76	968.293	−2.148	1	W2P2	
77	969.047	−1.458	1	W2Q3	blend
78	969.086	−2.095	1	L12P3	blend
79	970.560	−2.022	1	W2P3	
80	971.386	−1.460	1	W2Q4	
81	971.984	−1.705	1	L11R0	weak
82	973.348	−2.231	1	L11P1	
83	974.156	−1.903	1	L11R2	
84	975.343	−2.178	1	L11P2	weak
85	978.216	−2.175	1	L11P3	
86	981.441	−1.690	1	L10R0	
87	982.074	−1.876	1	L10R1	
88	982.834	−2.169	1	L10P1	
89	983.595	−1.950	1	L10R2	
90	984.866	−2.091	1	L10P2	
91	985.632	−1.157	1,2	W1R0	blend
92	985.651	−1.474	1,2	W1R1	blend
93	985.967	−2.108	1	L10R3	
94	986.246	−1.570	1	W1R2	
95	986.798	−1.439	1,2	W1Q1	
96	987.450	−1.578	1	W1R3	
97	987.770	−2.056	1	L10P3	
98	987.978	−1.440	1	W1Q2	
99	991.388	−1.939	1	W1P3	blend
100	991.394	−1.587	1	L9R0	blend
101	992.018	−1.441	1	W1Q4	blend
102	992.022	−1.745	1	L9R1	blend
103	992.052	−1.638	1	W1R5	blend
104	992.813	−2.116	1	L9P1	
105	993.492	−1.959	1	L10R5	blend, weak
106	993.549	−1.780	1	L9R2	blend
107	994.229	−1.885	1	W1P4	
108	994.876	−2.066	1	L9P2	blend
109	994.924	−1.442	1	W1Q5	blend
110	995.975	−1.793	1	L9R3	
111	997.829	−2.063	1,2	L9P3	see Add.
112	1001.826	−1.575	1	L8R0	
113	1002.457	−1.742	1,2	L8R1	
114	1003.304	−2.076	1	L8P1	
115	1003.989	−1.785	1	L8R2	
116	1005.397	−2.009	1	L8P2	
117	1006.346	−2.080	1	L9P5	blend
118	1006.418	−1.812	1	L8R3	blend
119	1008.392	−1.991	1	L8P3	blend

Table 2, continued ...

No.	λ [Å]	log(f)	VC	Transition	Remarks
120	1008.502	−1.672	1	W0R1	blend
121	1008.553	−1.349	1	W0R0	blend
122	1009.030	−1.783	1	W0R2	
123	1009.721	−2.866	1	L8R4	blend
124	1009.772	−1.623	1,2	W0Q1	blend
125	1010.132	−1.833	1	W0R3	
126	1010.941	−1.623	1	W0Q2	
127	1012.173	−2.276	1	W0P2	blend
128	1012.261	−1.983	1	L8P4	blend
129	1012.681	−1.625	1	W0Q3	
130	1012.822	−1.527	1	L7R0	
131	1013.434	−1.688	1,2	L7R1	blend
132	1013.480	−1.821	1	W0R5	blend
133	1014.334	−2.051	1	L7P1	
134	1014.509	−2.107	1	W0P3	
135	1014.977	−1.724	1	L7R2	blend
136	1014.980	−1.625	1	W0Q4	blend
137	1016.472	−1.996	1	L7P2	
138	1017.390	−2.036	1	W0P4	blend
139	1017.428	−1.735	1	L7R3	blend
140	1019.506	−1.991	1	L7P3	
141	1023.443	−1.996	1	L7P4	
142	1024.364	−1.540	1	L6R0	
143	1024.986	−1.703	1	L6R1	blend
144	1024.991	−1.842	1	L7R5	blend
145	1026.532	−1.740	1	L6R2	
146	1028.103	−1.983	1	L6P2	
147	1028.986	−1.752	1	L6R3	
148	1031.191	−1.966	1	L6P3	
149	1032.356	−1.757	1	L6R4	
150	1036.546	−1.567	1	L5R0	blend
151	1036.546	−1.836	1	L6R5	blend
152	1037.146	−1.733	1	L5R1	blend
153	1038.156	−2.068	1	L5P1	
154	1038.690	−1.770	1	L5R2	
155	1040.367	−2.001	1	L5P2	
156	1041.156	−1.785	1	L5R3	
157	1043.498	−1.983	1	L5P3	
158	1044.546	−1.791	1	L5R4	weak
159	1047.554	−1.979	1	L5P4	
160	1049.366	−1.629	1	L4R0	
161	1049.958	−1.796	1	L4R1	
162	1051.031	−2.125	1	L4P1	
163	1051.497	−1.833	1	L4R2	
164	1053.281	−2.056	1	L4P2	
165	1053.976	−1.848	1	L4R3	
166	1056.469	−2.037	1	L4P3	
167	1057.379	−1.854	1	L4R4	weak
168	1060.580	−2.032	1	L4P4	weak
169	1062.883	−1.740	1	L3R0	blend
170	1063.460	−1.907	1	L3R1	
171	1064.606	−2.234	1	L3P1	
172	1064.995	−1.947	1	L3R2	
173	1066.900	−2.163	1	L3P2	
174	1067.478	−1.963	1	L3R3	
175	1070.142	−2.142	1	L3P3	
176	1077.138	−1.924	1	L2R0	
177	1077.698	−2.092	1	L2R1	
178	1078.925	−2.415	1	L2P1	
179	1079.226	−2.132	1	L2R2	
180	1081.265	−2.344	1	L2P2	
181	1081.710	−2.147	1	L2R3	blend
182	1084.559	−2.321	1	L2P3	
183	1092.194	−2.225	1	L1R0	
184	1092.732	−2.395	1	L1R1	
185	1093.955	−2.310	1	L2P5	weak
186	1094.052	−2.714	1	L1P1	
187	1094.244	−2.436	1	L1R2	
188	1096.439	−2.642	1	L1P2	
189	1096.725	−2.451	1	L1R3	blend
190	1099.788	−2.620	1	L1P3	
191	1100.165	−2.460	1	L1R4	weak
192	1108.128	−2.762	1	L0R0	
193	1108.634	−2.932	1	L0R1	
194	1110.063	−3.250	1	L0P1	blend
195	1110.120	−2.971	1	L0R2	blend
196	1112.495	−3.177	1	L0P2	blend
197	1112.584	−2.991	1	L0R3	blend
198	1115.896	−3.153	1	L0P3	

Table 2, continued ...

3.3. Interstellar metal lines

Most of the metal lines can be observed in both interstellar components with the second component being only slightly weaker than the main component. High resolution spectra do show more components (Spitzer & Fitzpatrick 1993), but in the *ORFEUS* echelle spectra only two well separated components are seen. The separation is best seen in the Ar I lines λ1048 and λ1067 and the N I triplett λ1134. Interstellar O VI at λ1032 and λ1037 appears quite broad. Widmann estimated a $N(O\,VI) = (0.99 \pm 0.15)\,10^{14}\,\mathrm{cm}^{-2}$ from these *ORFEUS* echelle spectra (Widmann et al. 1998; Widmann 1999).

Table 3. Table of identified interstellar metal lines. For unresolved doublets and triplets an average wavelength and a calculated effective log(gf) are given. VC is the velocity component as given in Table 1.

No.	λ [Å]	log(gf)	VC	Elem.	Remarks
199	919.658	−2.391	1,2	O I	triplet, blend
200	924.952	−2.099	1,2	O I	triplet
201	925.442	−2.752	1,2	O I	comp. 2 ?
202	926.212	−0.359	1,2	Fe II	blend
203	929.517	−1.928	1,2	O I	triplet, blend
204	930.257	−2.571	1,2	O I	weak
205	936.629	−1.729	1,2	O I	triplet
206	945.191	−0.565	1,2	C I	weak
207	946.978	−0.230	1,2	S II	blend
208	948.686	−1.492	1,2	O I	triplet, blend
209	950.112	−1.714	1	O I*	doublet, blend
210	950.885	−2.105	1,2	O I	blend
211	952.303	−2.152	1,2	N I	blend
212	952.415	−2.206	1,2	N I	blend

Table 3, continued ...

No.	λ [Å]	$\log(gf)$	VC	Elem.	Remarks
213	953.415	−1.371	1,2	N I	blend
214	953.655	−1.090	1,2	N I	blend
215	953.970	−0.983	1,2	N I	blend
216	954.104	−1.752	1,2	N I	blend
217	961.041	−0.457	1,2	P II	weak
218	963.801	0.164	1,2	P II	blend
219	963.990	−1.134	1,2	N I	comp.2 blend
220	964.626	−1.326	1,2	N I	
221	965.041	−1.634	1,2	N I	blend
222	971.738	−1.131	1,2	O I	triplet
223	977.020	−0.118	1	C III	blend
224	1020.699	−1.248	1,2	Si II	
225	1031.926	−0.575	1,2	O VI	
226	1036.337	−0.609	1,2	C II	
227	1037.018	−0.308	1,2	C II*	blend
228	1037.617	−0.879	1,2	O VI	blend
229	1039.230	−1.337	1,2	O I	
230	1048.220	−0.612	1,2	Ar I	
231	1055.262	−1.097	1,2	Fe II	weak
232	1063.176	−0.222	1,2	Fe II	blend
233	1063.972	−1.347	1,2	Fe II	weak
234	1066.660	−1.177	1,2	Ar I	
235	1081.875	−0.854	1,2	Fe II	blend
236	1083.990	−0.987	1,2	N II	
237	1096.877	−0.495	1,2	Fe II	blend
238	1112.048	−1.040	1,2	Fe II	weak, blend
239	1121.975	−0.699	1,2	Fe II	
240	1122.526	−0.149	1,2	Fe III	
241	1125.448	−0.959	1,2	Fe II	
242	1133.665	−1.222	1,2	Fe II	
243	1134.165	−1.270	1,2	N I	comp.1 blend
244	1134.415	−0.969	1,2	N I	comp.2 blend
245	1134.980	−0.793	1,2	N I	
246	1143.226	−0.876	1,2	Fe II	
247	1144.938	0.021	1,2	Fe II	
248	1152.818	−0.627	1,2	P II	
249	1190.416	−0.301	1,2	Si II	
250	1193.290	−0.001	1,2	Si II	
251	1199.550	−0.275	1,2	N I	
252	1200.223	−0.451	1,2	N I	
253	1200.710	−0.752	1,2	N I	
254	1206.500	0.223	1,2	Si III	blend
255	1250.584	−1.661	1,2	S II	
256	1253.811	−1.361	1,2	S II	
257	1259.519	−1.187	1,2	S II	
258	1260.422	0.304	1,2	Si II	blend
259	1260.533	−0.602	1,2	Fe II	blend
260	1277.245	−1.015	1	C I	weak
261	1302.168	−0.612	1,2	O I	
262	1304.370	−0.531	1,2	Si II	
263	1334.532	−0.593	1,2	C II	
264	1335.690	−0.292	1,2	C II*	doublet

3.4. Lyman series lines

Of the Lyman series 14 lines are detectable, from which the lines below the $\lambda 915.824$ line are not separated, so that this line marks the interstellar Lyman limit towards HD 93521.

Table 4. Table of the identified interstellar Lyman-series (H I). All lines are doublets with a maximum separation of 5.4 mÅ (at $\lambda 1216$). The resulting wavelength and $\log(gf)$ is given. VC is the velocity component as given in Table 1.

No.	λ [Å]	$\log(gf)$	VC	Lyman Name	Remarks
265	915.824	−3.029	1	14	
266	916.429	−2.938	1	13	
267	917.181	−2.840	1	12	
268	918.129	−2.735	1	11	
269	919.351	−2.620	1	10	
270	920.963	−2.493	1	9	
271	923.150	−2.353	1	8	
272	926.226	−2.196	1	7	
273	930.748	−2.016	1	6	
274	937.803	−1.807	1	ϵ	
275	949.743	−1.555	1	δ	
276	972.537	−1.237	1	γ	
277	1025.722	−0.801	1	β	
278	1215.670	−0.079	1	α	
279	1215.670	−0.079	4	α	geocoronal

3.5. Stellar lines

The two N V-lines at $\lambda\lambda 1239/1243$ have a pronounced P-Cygni profile. Within the absorption part both lines show two significant narrow absorption components at -270 and $-340\,\mathrm{km\,s^{-1}}$. These narrow absorption components could be an indication for a disk in the wind of HD 93521 (Bjorkman et al. 1994). The same components are also visible in the Si IV doublet at $\lambda\lambda 1394/1403$, in Si IV $\lambda 1073$ and in Si III $\lambda 1206$.

The strong Si III $\lambda\lambda 1300$ triplets are seen as wind absorption lines (Massa 1995). They appear at a range between $-60\,\mathrm{km\,s^{-1}}$ and $-100\,\mathrm{km\,s^{-1}}$, whereas Massa reports a value of $-30\,\mathrm{km\,s^{-1}}$. This difference could be due to some long term wind variability.

The comparatively strong stellar absorption at 1085 Å could not be clearly identified, it is possibly a superposition of different lines. A candidate is the He II $\lambda 1084.9$ line, but as the next lower unblended He II line at $\lambda 958.7$ is rather weak, the identification is not sure. There is a Fe II resonance line at $\lambda 1085.0$ with a low $\log(gf) = -2.106$, but also non-resonance lines of Fe II and Fe III are present in this region. So this line probably requires a more detailed analysis.

Table 5. Table of identified stellar (*) and stellar wind (w) lines. For the N III doublets only the stronger of the two lines is listed. VC is the velocity component as given in Table 1.

No.	λ [Å]	$\log(gf)$	VC	Elem.	Remarks
280	977.020	−0.118	3	C III (*)	
281	979.832	−0.248	3	N III* (*)	doublet
282	979.905	−0.055	3	N III* (*)	doublet

Table 5, continued ...

No.	λ [Å]	$\log(gf)$	VC	Elem.	Remarks
283	989.799	−0.671	3	N III (*)	
284	989.873	−0.575	3	Si II (*)	
285	1031.926	−0.575	3	O VI (*)	P Cygni
286	1037.617	−0.879	3	O VI (*)	P Cygni
287	1062.662	−1.097	3	S IV (*)	
288	1072.974	−0.846	3,5,6	S IV* (*)	
289	1073.516	−1.800	3	S IV* (*)	
290	1117.977	−0.024	3	P V (*)	
291	1128.008	−0.329	3	P V (*)	
292	1174.933	−0.459	3	C III* (*)	
293	1175.263	−0.549	3	C III* (*)	
294	1175.590	−0.679	3	C III* (*)	
295	1175.711	0.021	3	C III* (*)	
296	1175.987	−0.549	3	C III* (*)	
297	1176.370	−0.459	3	C III* (*)	
298	1183.032	−0.591	3	N III* (*)	doublet
299	1184.514	−0.195	3	N III* (*)	doublet
300	1206.500	0.223	3,5,6	Si III (*)	
301	1238.821	−0.503	3,5,6	N V (*)	
302	1242.804	−0.806	3,5,6	N V (*)	
303	1247.383	−0.157	3	C III (*)	
304	1294.545	−0.037	7	Si III* (w)	
305	1296.726	−0.127	7	Si III* (w)	
306	1298.892	−0.257	7	Si III* (w)	
307	1298.946	0.443	7	Si III* (w)	
308	1301.149	−0.127	7	Si III* (w)	
309	1303.323	−0.037	7	Si III* (w)	
310	1393.755	0.012	3,5,6	Si IV (*)	
311	1402.770	−0.292	3,5,6	Si IV (*)	

4. Conclusions

The presented *ORFEUS II* Echelle spectrum of HD 93521 shows an extraordinary rich variety of very sharp interstellar absorption lines, especially in the wavelength region between 900 Å and 1200 Å, which was not very well studied before the two *ORFEUS* missions and for which only now new observation possibilities exist. Particularly the nearly complete presence of very sharp (FWHM $\approx$ 100 mÅ) H_2 absorption lines in this spectrum – which will be analysed in detail in a forthcoming paper – makes it well suited as a reference spectrum for interstellar molecular hydrogen. Molecular hydrogen is partially visible in the interstellar high velocity component too. Additionally some stellar lines show narrow absorption components wich are varying in time and which could be an indication for a disk.

Acknowledgements. ORFEUS could only be realized with the support of all our German and American colleagues and collaborators. The authors wish to thank Philipp Richter and Klaas S. de Boer for helpful discussions. The ORFEUS program was supported by DARA grants WE3 OS 8501 and WE2 QV 9304 and NASA grant NAG5-696.

References

Abgrall H., Roueff E., Launnay F., Roncin J.-Y., Subtil J.-L., 1993, A&AS 101, 273

Barnstedt J., Kappelmann N., Appenzeller I., et al., 1999, A&AS 134, 561

Bjorkman J.E., Ignace R., Tripp T.M., Cassinelli J.P., 1994, ApJ 435, 416

Feibelman W.A., Johannson S., 1995, ApJS 100, 405

Grewing M., Boksenberg A., Savage B.D., et al., 1978, Nature 275, 394

Irvine N.J., 1989, ApJ 337, L33

Keenan F.P., Shaw C.R., Bates B., Dufton P.L., Kemp S.N., 1995, MNRAS 272, 599

Kelly R.L., 1968, *Atomic Emission Lines Below 2000 Angstroms, Hydrogen Through Argon*, Naval Research Laboratory, Washington D.C. (see also http://cfa-www.harvard.edu/amdata/ampdata/kelly/kelly.html)

Kurucz R.L., 1995, CD No. 23, (http://www.pmp.uni-hannover.de/projekte/kurucz/sekur.html)

Lennon D.J., Dufton P.L., Keenan F.P., Holmgren D.E., 1991, A&A 246, 175

Massa D., 1995, ApJ 438, 376

Morton D.C., Dinerstein H.L., 1976, ApJ 204, 1

Morton D.C., 1991, ApJS 77, 119

Ramella M., Morossi C., Santin P., 1980, A&A 90, 146

Savage B.D., Bohlin R.C., Drake J.F., Budich W., 1977, ApJ 216, 291

Spitzer L., Fitzpatrick E.L., 1992, ApJ 391, L41

Spitzer L., Fitzpatrick E.L., 1993, ApJ 409, 299

Widmann H., de Boer K.S., Richter P., Krämer G., et al., 1998, A&A 338, L1

Widmann H., *ORFEUS II–Echelle-Spektren, Untersuchungen des heißen galaktischen Halos*, Ph.D. Thesis, Universität Tübingen, 1999

Appendix: plots of the spectrum of HD 93521

The following plots show the complete ORFEUS II Echelle spectrum of HD 93521. The numbers shown in squared brackets correspond to the running numbers given in the Tables 2 - 5. Stellar lines are marked as (*), stellar wind lines as (w). Non-resonance lines are additionally marked with an asterisk, *.

The plots show one Echelle order per plot for wavelengths above 1130 Å (Echelle orders 40 to 49), and half an Echelle order per plot for Echelle orders 50 to 61 ($\lambda < 1130$ Å) which includes all H_2-lines. Thus the wavelength scale changes from order to order, but the relative wavelength scale (radial velocity scale) is nearly constant within these two wavelength ranges.

Addendum

H_2-line λ997.829 (no. 111) was erroneously identified with two velocity components. The more probable identification for the weaker component however is the H_2-line λ997.640 W1P5 with $\log(f) = -1.921$.

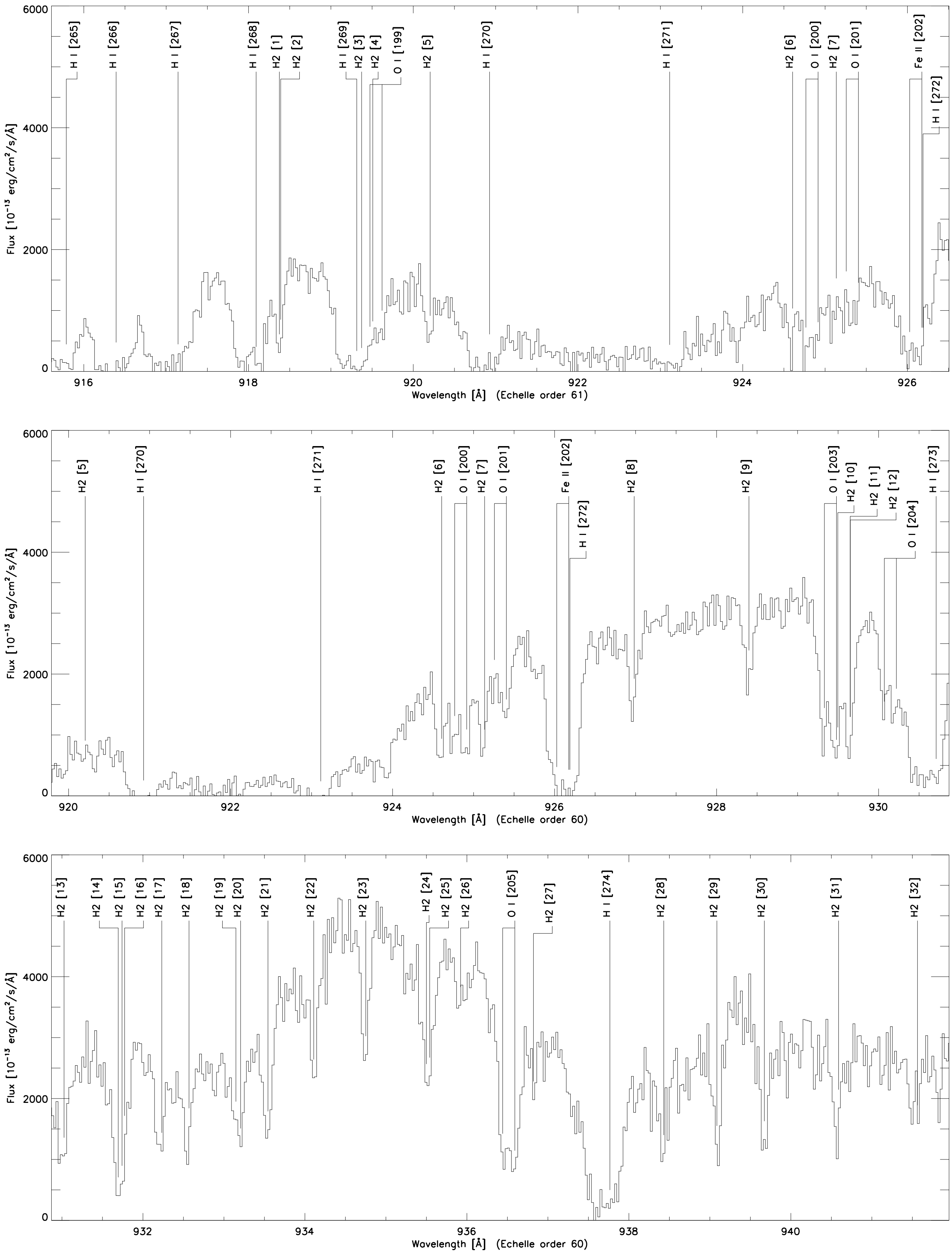
H I [265]
H I [266]
H I [267]
H I [268]
H2 [1]
H2 [2]
H I [269]
H2 [3]
H2 [4]
O I [199]
H2 [5]
H I [270]
H I [271]
H2 [6]
O I [200]
H2 [7]
O I [201]
Fe II [202]
H I [272]
Flux [10^{-13} erg/cm^2/s/Å]
Wavelength [Å] (Echelle order 61)
H2 [5]
H I [270]
H I [271]
H2 [6]
O I [200]
H2 [7]
O I [201]
Fe II [202]
H I [272]
H2 [8]
H2 [9]
O I [203]
H2 [10]
H2 [11]
H2 [12]
O I [204]
H I [273]
Flux [10^{-13} erg/cm^2/s/Å]
Wavelength [Å] (Echelle order 60)
H2 [13]
H2 [14]
H2 [15]
H2 [16]
H2 [17]
H2 [18]
H2 [19]
H2 [20]
H2 [21]
H2 [22]
H2 [23]
H2 [24]
H2 [25]
H2 [26]
O I [205]
H2 [27]
H I [274]
H2 [28]
H2 [29]
H2 [30]
H2 [31]
H2 [32]
Flux [10^{-13} erg/cm^2/s/Å]
Wavelength [Å] (Echelle order 60)

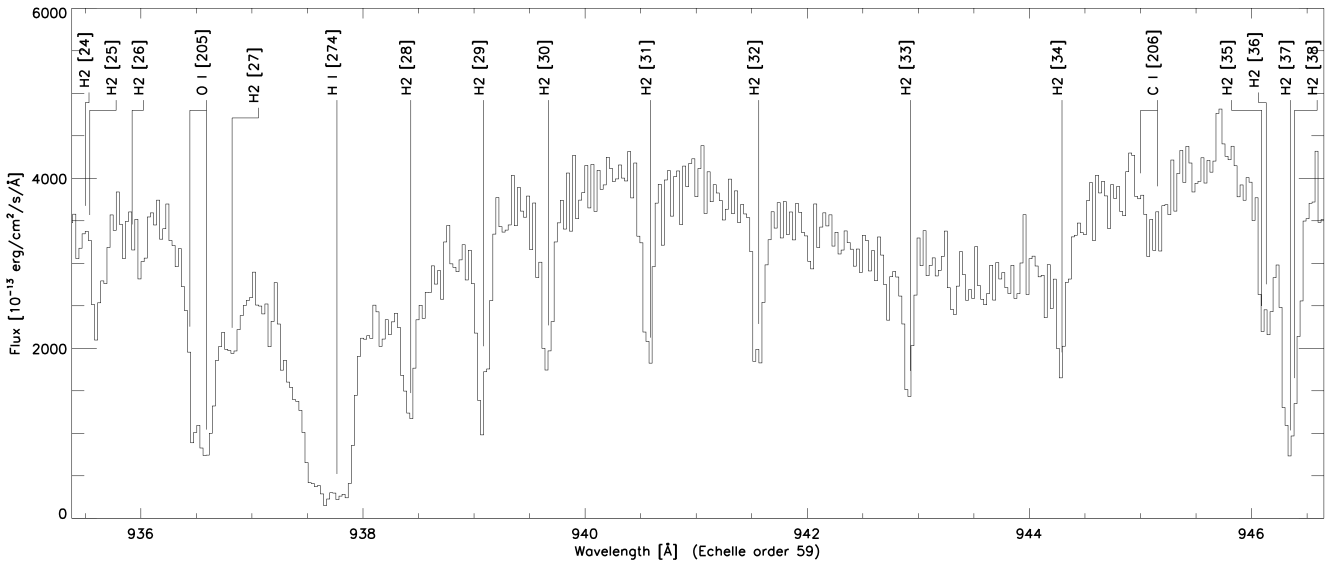
H2 [24]
H2 [25]
H2 [26]
O I [205]
H2 [27]
H I [274]
H2 [28]
H2 [29]
H2 [30]
H2 [31]
H2 [32]
H2 [33]
H2 [34]
C I [206]
H2 [35]
H2 [36]
H2 [37]
H2 [38]
Flux [10^{-13} erg/cm²/s/Å]
6000
4000
2000
0
936
938
940
942
944
946
Wavelength [Å] (Echelle order 59)

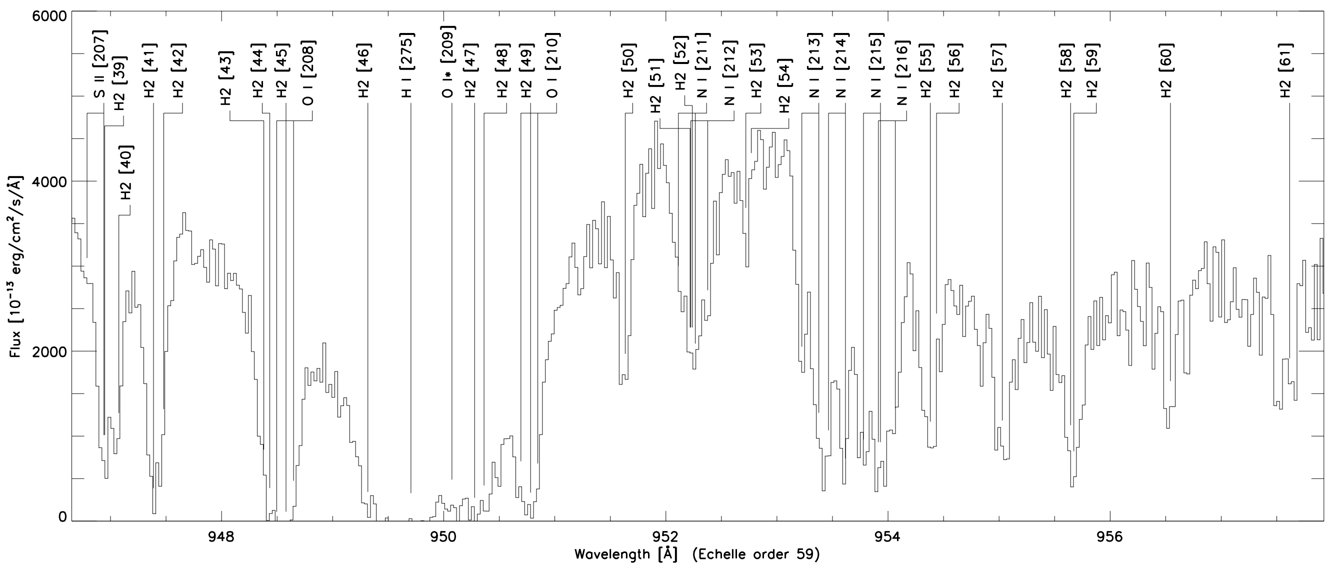
S II [207]
H2 [39]
H2 [40]
H2 [41]
H2 [42]
H2 [43]
H2 [44]
H2 [45]
O I [208]
H2 [46]
H I [275]
O I• [209]
H2 [47]
H2 [48]
H2 [49]
O I [210]
H2 [50]
H2 [51]
H2 [52]
N I [211]
N I [212]
H2 [53]
H2 [54]
N I [213]
N I [214]
N I [215]
N I [216]
H2 [55]
H2 [56]
H2 [57]
H2 [58]
H2 [59]
H2 [60]
H2 [61]
Flux [10^{-13} erg/cm²/s/Å]
6000
4000
2000
0
948
950
952
954
956
Wavelength [Å] (Echelle order 59)

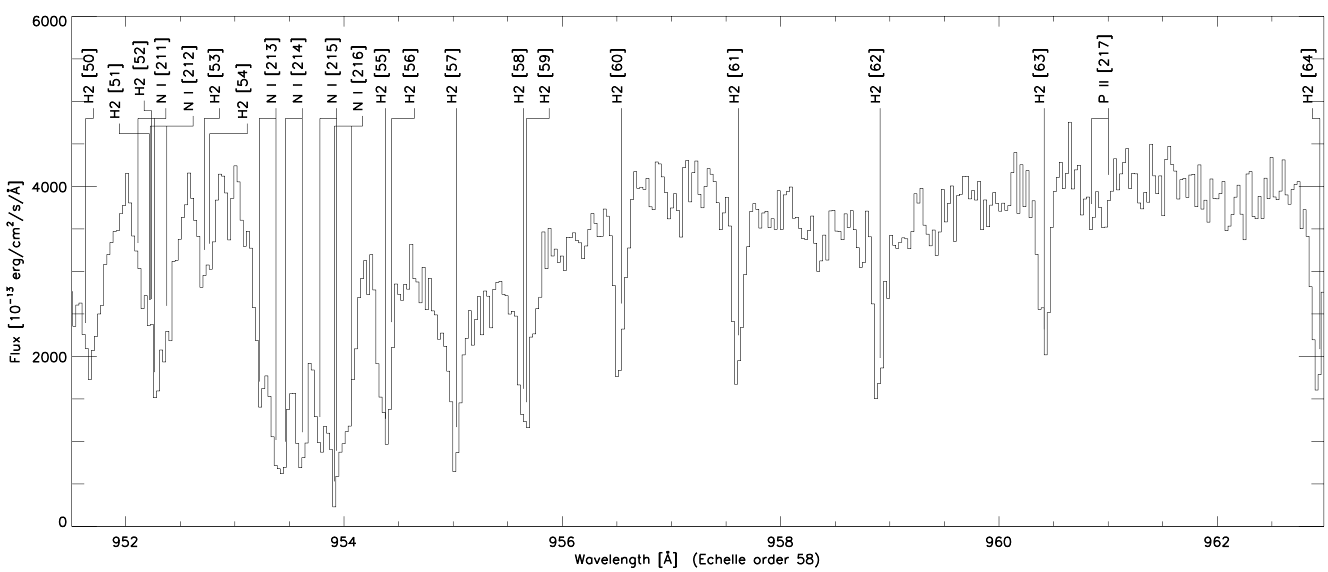
H2 [50]
H2 [51]
H2 [52]
N I [211]
N I [212]
H2 [53]
H2 [54]
N I [213]
N I [214]
N I [215]
N I [216]
H2 [55]
H2 [56]
H2 [57]
H2 [58]
H2 [59]
H2 [60]
H2 [61]
H2 [62]
H2 [63]
P II [217]
H2 [64]
Flux [10^{-13} erg/cm²/s/Å]
6000
4000
2000
0
952
954
956
958
960
962
Wavelength [Å] (Echelle order 58)

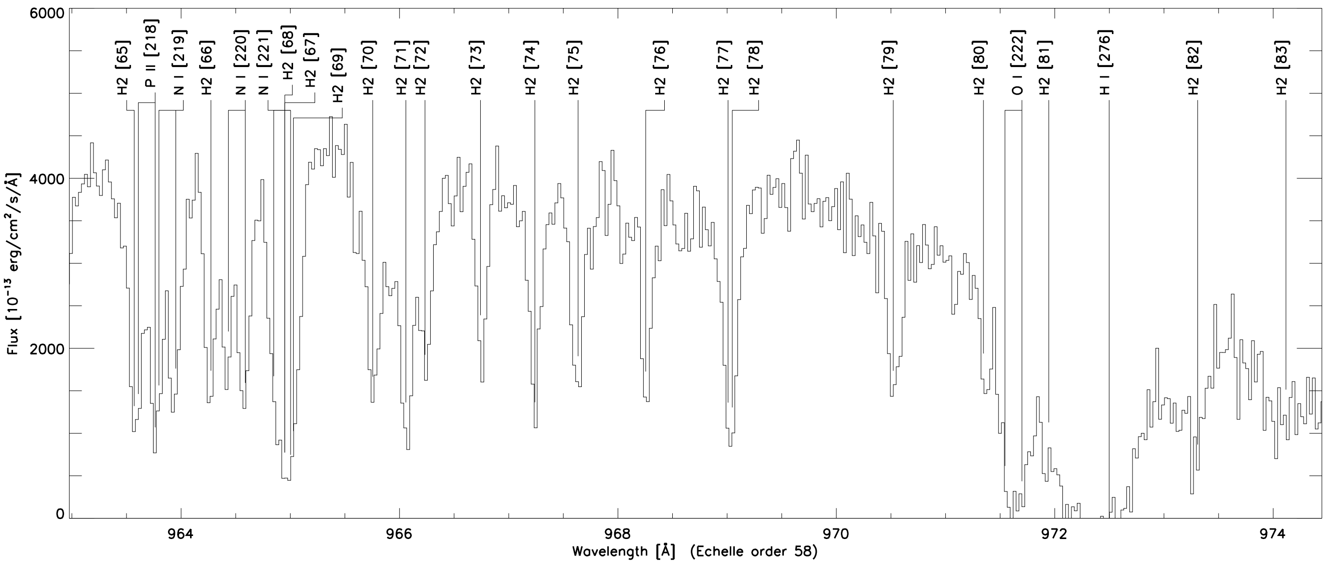
H2 [65]
P II [218]
N I [219]
H2 [66]
N I [220]
N I [221]
H2 [68]
H2 [67]
H2 [69]
H2 [70]
H2 [71]
H2 [72]
H2 [73]
H2 [74]
H2 [75]
H2 [76]
H2 [77]
H2 [78]
H2 [79]
H2 [80]
O I [222]
H2 [81]
H I [276]
H2 [82]
H2 [83]
Flux [10⁻¹³ erg/cm²/s/Å]
Wavelength [Å] (Echelle order 58)

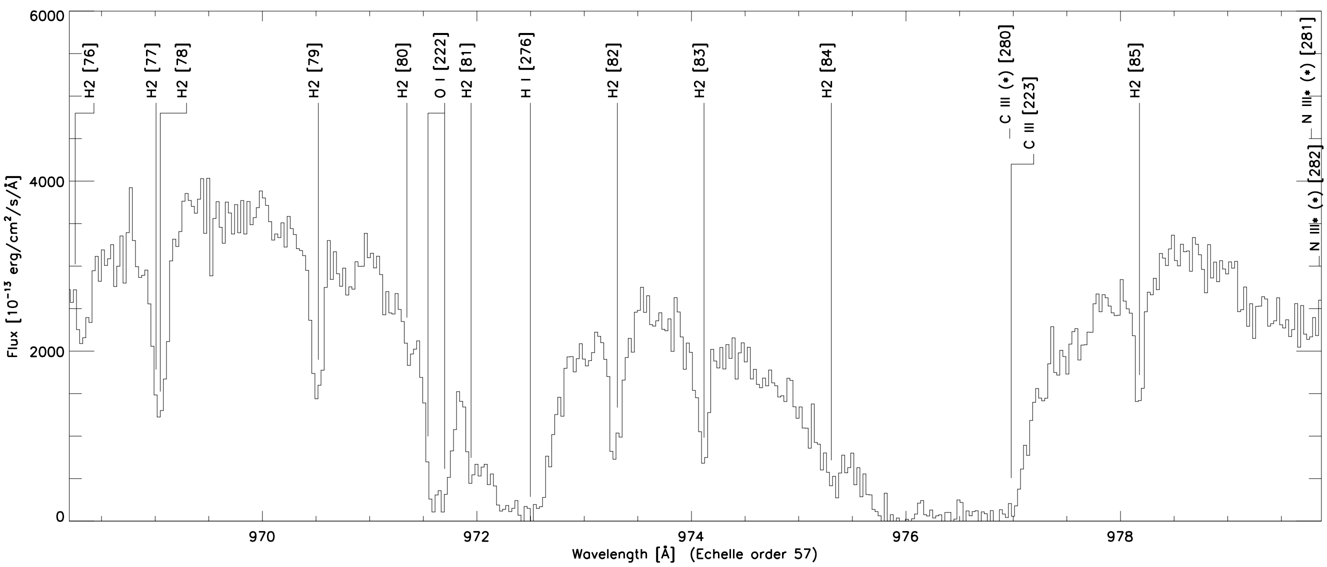
H2 [76]
H2 [77]
H2 [78]
H2 [79]
H2 [80]
O I [222]
H2 [81]
H I [276]
H2 [82]
H2 [83]
H2 [84]
C III (•) [280]
C III [223]
H2 [85]
N III• (•) [281]
N III• (•) [282]
Flux [10⁻¹³ erg/cm²/s/Å]
Wavelength [Å] (Echelle order 57)

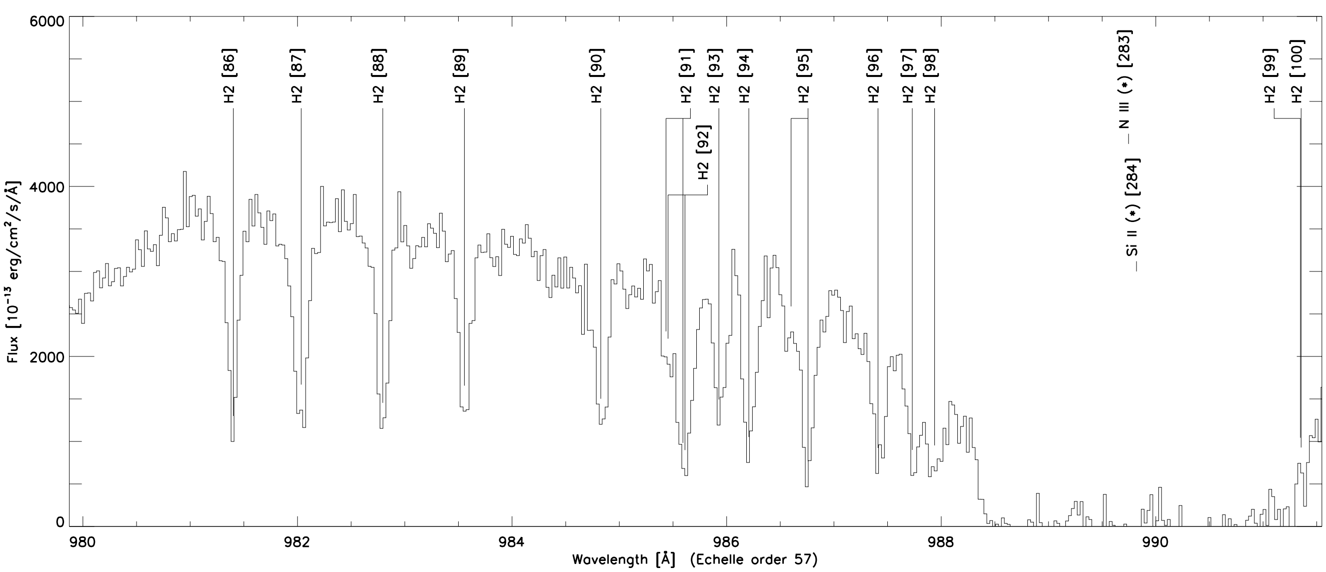
H2 [86]
H2 [87]
H2 [88]
H2 [89]
H2 [90]
H2 [91]
H2 [92]
H2 [93]
H2 [94]
H2 [95]
H2 [96]
H2 [97]
H2 [98]
N III (•) [283]
Si II (•) [284]
H2 [99]
H2 [100]
Flux [10⁻¹³ erg/cm²/s/Å]
Wavelength [Å] (Echelle order 57)

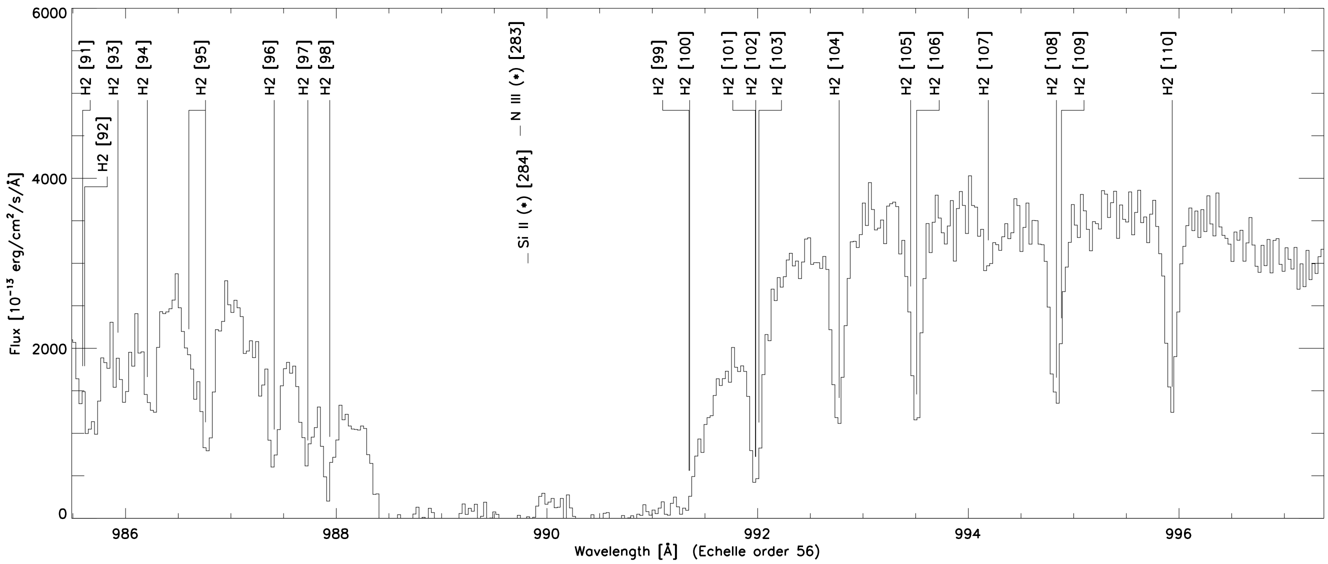
H2 [91]
H2 [92]
H2 [93]
H2 [94]
H2 [95]
H2 [96]
H2 [97]
H2 [98]
Si II (*) [284]
N III (*) [283]
H2 [99]
H2 [100]
H2 [101]
H2 [102]
H2 [103]
H2 [104]
H2 [105]
H2 [106]
H2 [107]
H2 [108]
H2 [109]
H2 [110]
Flux [10^-13 erg/cm^2/s/Å]
Wavelength [Å] (Echelle order 56)

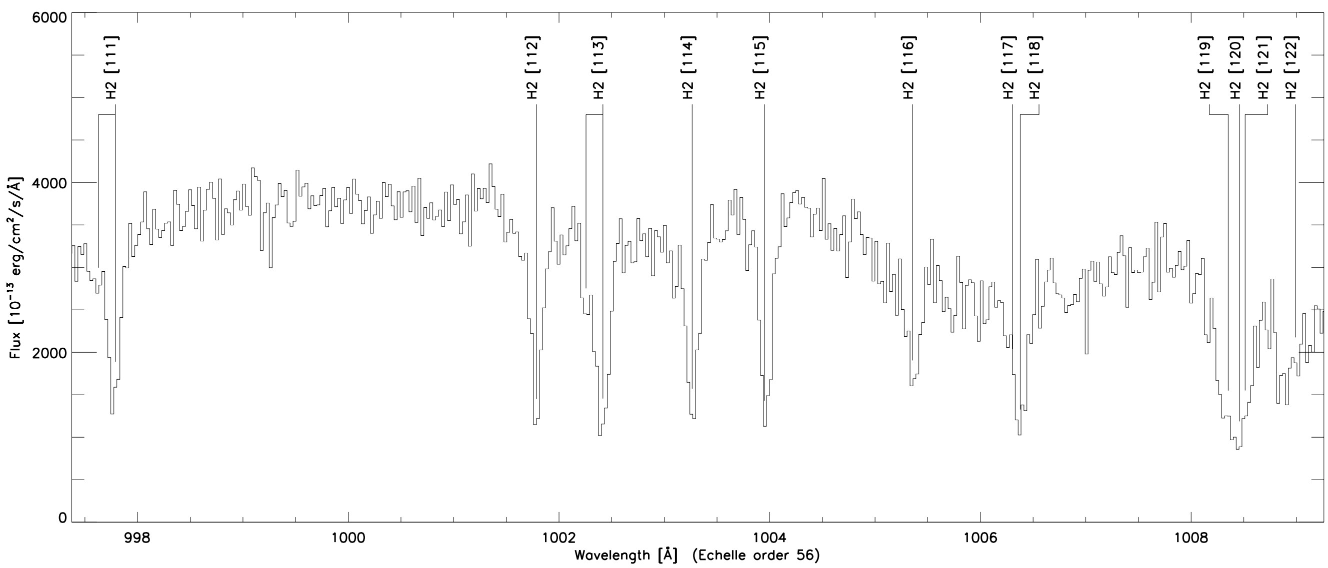
H2 [111]
H2 [112]
H2 [113]
H2 [114]
H2 [115]
H2 [116]
H2 [117]
H2 [118]
H2 [119]
H2 [120]
H2 [121]
H2 [122]
Flux [10^-13 erg/cm^2/s/Å]
Wavelength [Å] (Echelle order 56)

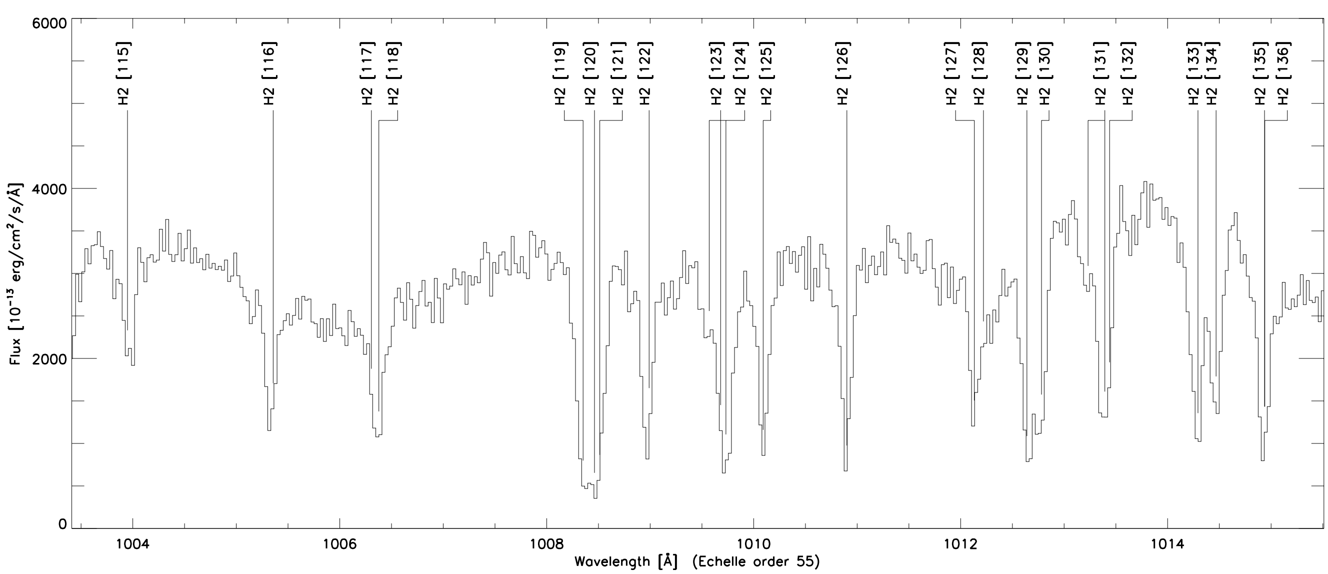
H2 [115]
H2 [116]
H2 [117]
H2 [118]
H2 [119]
H2 [120]
H2 [121]
H2 [122]
H2 [123]
H2 [124]
H2 [125]
H2 [126]
H2 [127]
H2 [128]
H2 [129]
H2 [130]
H2 [131]
H2 [132]
H2 [133]
H2 [134]
H2 [135]
H2 [136]
Flux [10^-13 erg/cm^2/s/Å]
Wavelength [Å] (Echelle order 55)

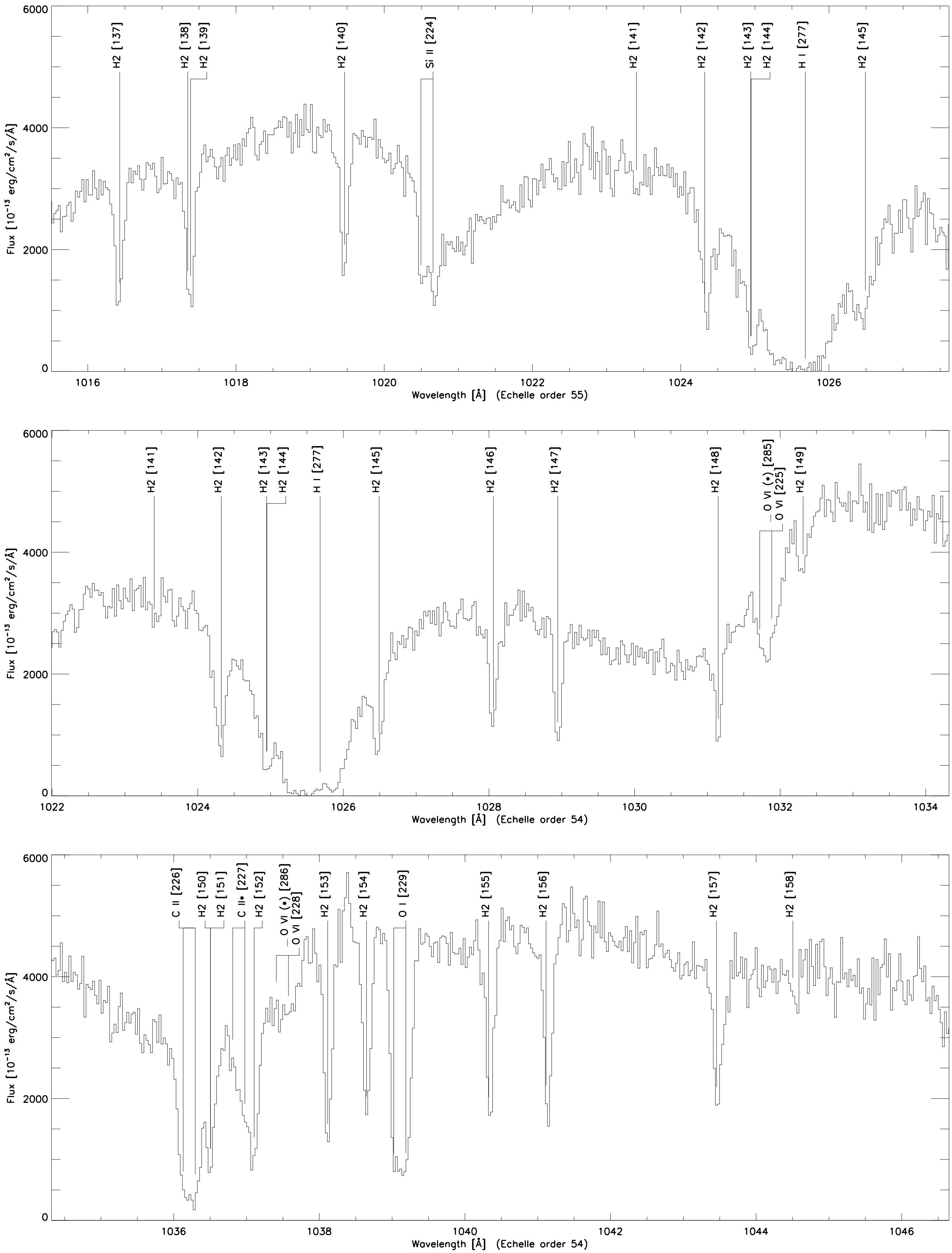
H2 [137]
H2 [138]
H2 [139]
H2 [140]
Si II [224]
H2 [141]
H2 [142]
H2 [143]
H2 [144]
H I [277]
H2 [145]
Flux [10⁻¹³ erg/cm²/s/Å]
Wavelength [Å] (Echelle order 55)
H2 [146]
H2 [147]
H2 [148]
O VI (*) [285]
O VI [225]
H2 [149]
Wavelength [Å] (Echelle order 54)
C II [226]
H2 [150]
H2 [151]
C II* [227]
H2 [152]
O VI (*) [286]
O VI [228]
H2 [153]
H2 [154]
O I [229]
H2 [155]
H2 [156]
H2 [157]
H2 [158]
Wavelength [Å] (Echelle order 54)

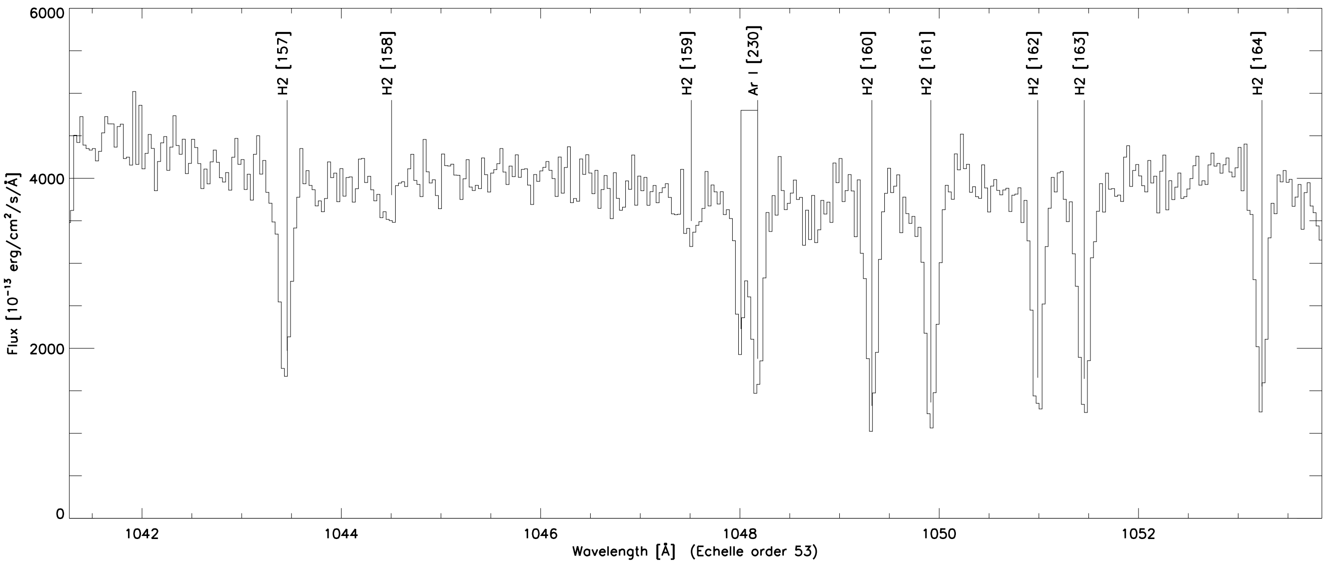
H2 [157]
H2 [158]
H2 [159]
Ar I [230]
H2 [160]
H2 [161]
H2 [162]
H2 [163]
H2 [164]
Flux [10⁻¹³ erg/cm²/s/Å]
Wavelength [Å] (Echelle order 53)

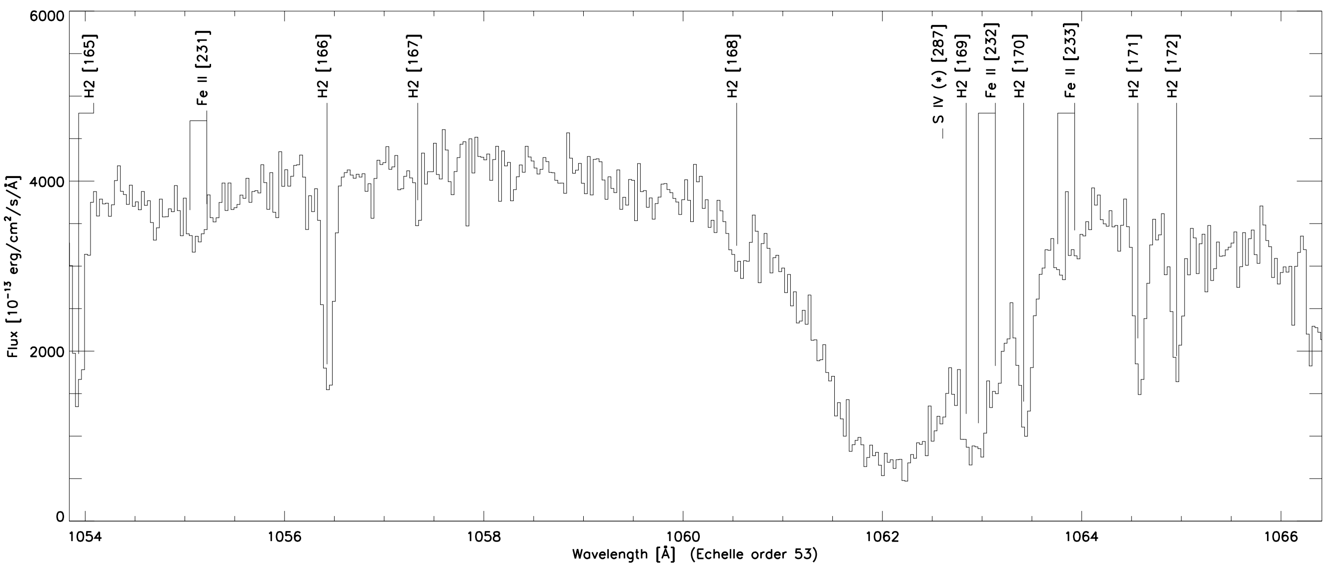
H2 [165]
Fe II [231]
H2 [166]
H2 [167]
H2 [168]
S IV (•) [287]
H2 [169]
Fe II [232]
H2 [170]
Fe II [233]
H2 [171]
H2 [172]
Flux [10⁻¹³ erg/cm²/s/Å]
Wavelength [Å] (Echelle order 53)

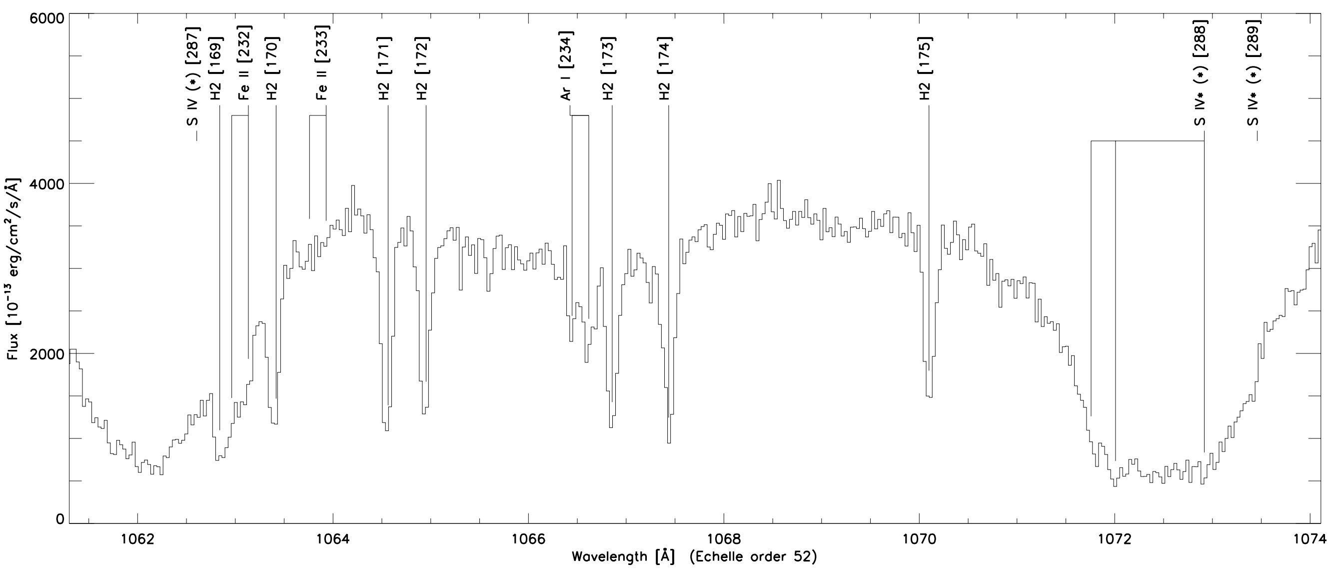
S IV (•) [287]
H2 [169]
Fe II [232]
H2 [170]
Fe II [233]
H2 [171]
H2 [172]
Ar I [234]
H2 [173]
H2 [174]
H2 [175]
S IV• (•) [288]
S IV• (•) [289]
Flux [10⁻¹³ erg/cm²/s/Å]
Wavelength [Å] (Echelle order 52)

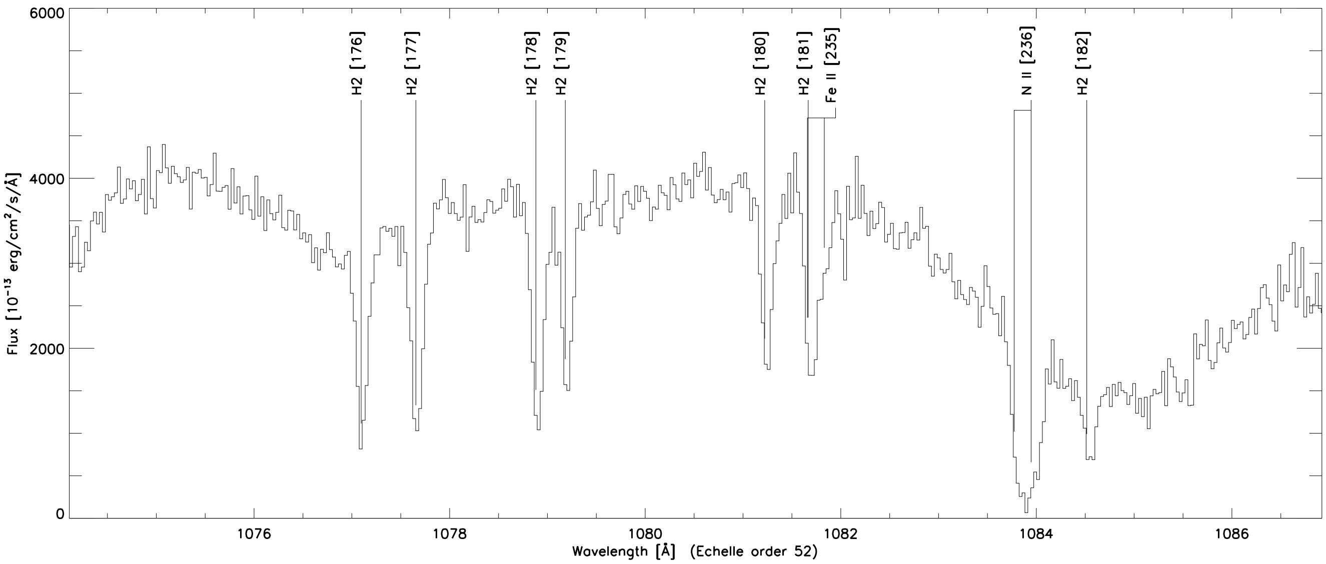
H2 [176]
H2 [177]
H2 [178]
H2 [179]
H2 [180]
H2 [181]
Fe II [235]
N II [236]
H2 [182]
Flux [10^-13 erg/cm^2/s/Å]
6000
4000
2000
0
1076
1078
1080
1082
1084
1086
Wavelength [Å] (Echelle order 52)

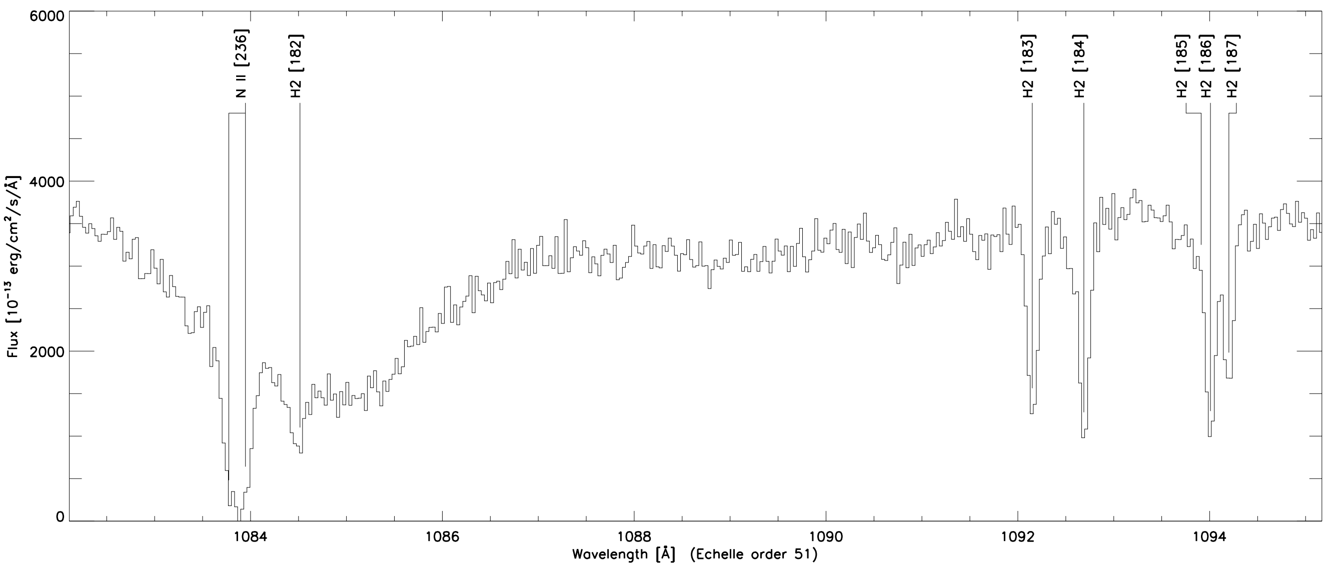
N II [236]
H2 [182]
H2 [183]
H2 [184]
H2 [185]
H2 [186]
H2 [187]
Flux [10^-13 erg/cm^2/s/Å]
6000
4000
2000
0
1084
1086
1088
1090
1092
1094
Wavelength [Å] (Echelle order 51)

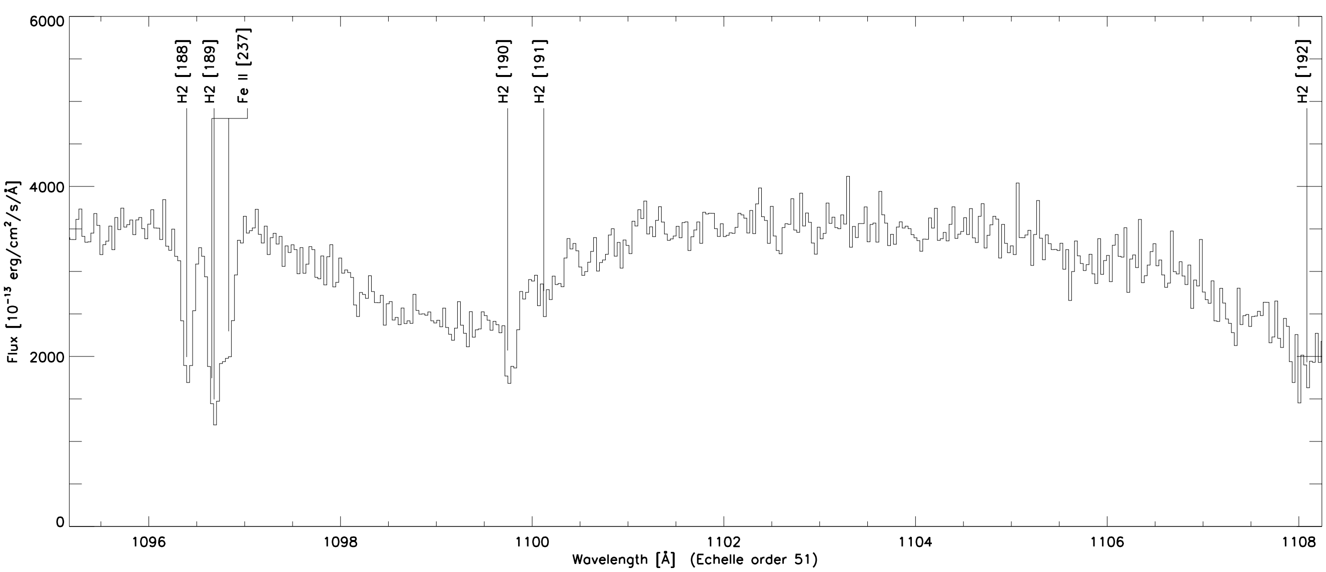
H2 [188]
H2 [189]
Fe II [237]
H2 [190]
H2 [191]
H2 [192]
Flux [10^-13 erg/cm^2/s/Å]
6000
4000
2000
0
1096
1098
1100
1102
1104
1106
1108
Wavelength [Å] (Echelle order 51)

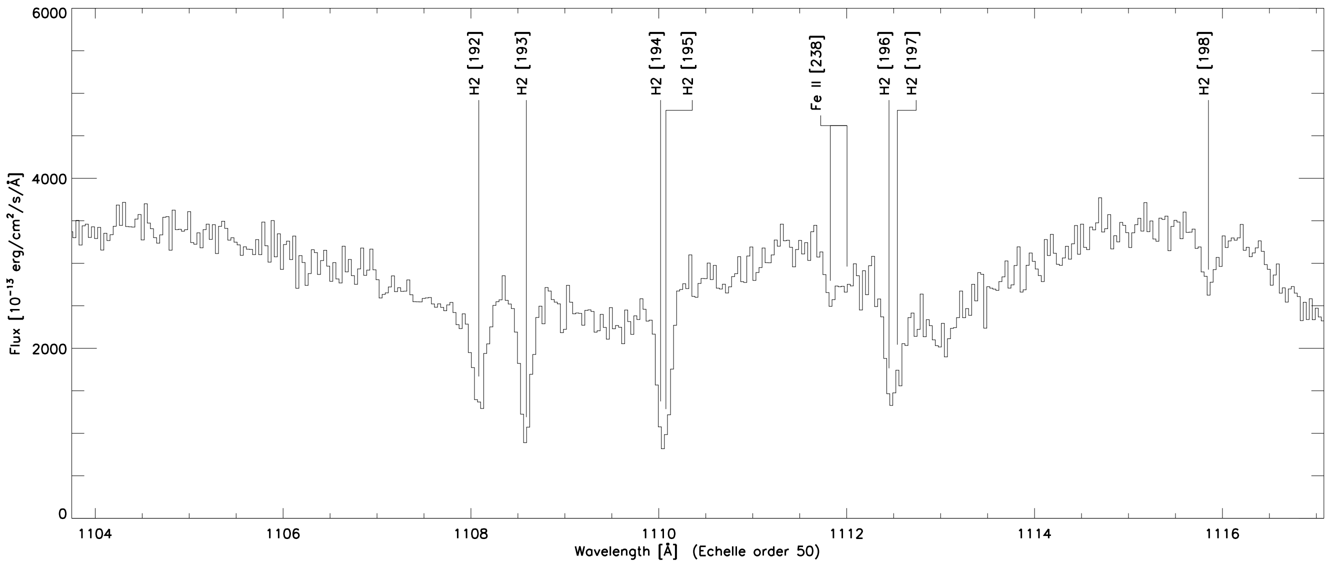
H2 [192]
H2 [193]
H2 [194]
H2 [195]
Fe II [238]
H2 [196]
H2 [197]
H2 [198]
Flux [10⁻¹³ erg/cm²/s/Å]
Wavelength [Å] (Echelle order 50)

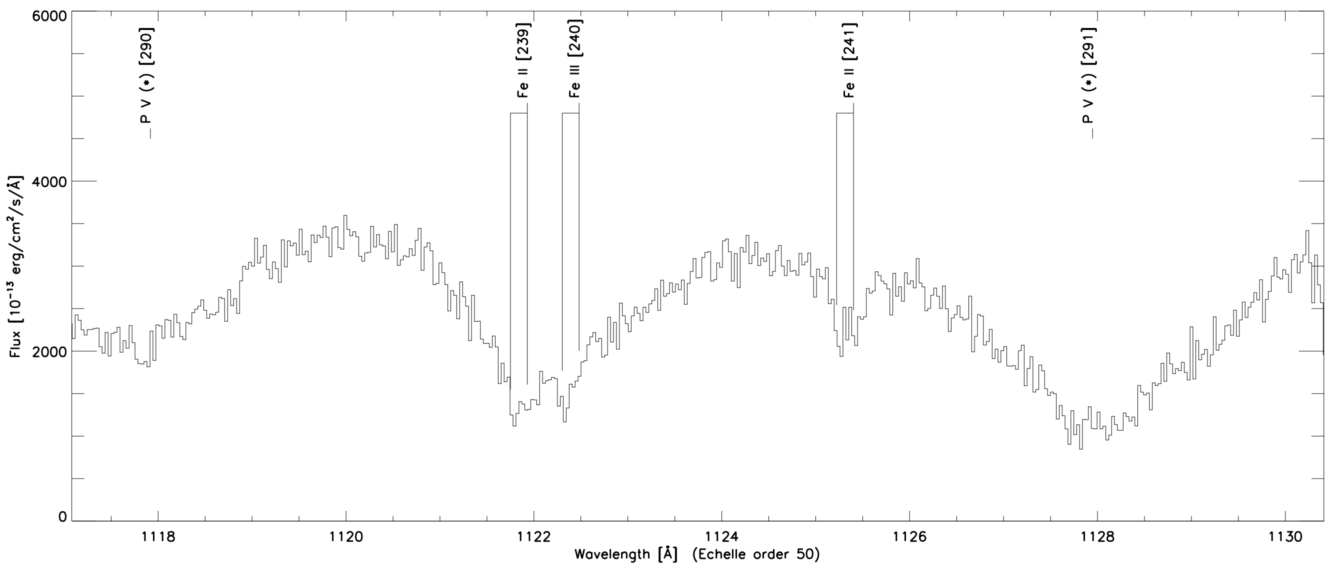
P V (*) [290]
Fe II [239]
Fe III [240]
Fe II [241]
P V (*) [291]
Flux [10⁻¹³ erg/cm²/s/Å]
Wavelength [Å] (Echelle order 50)

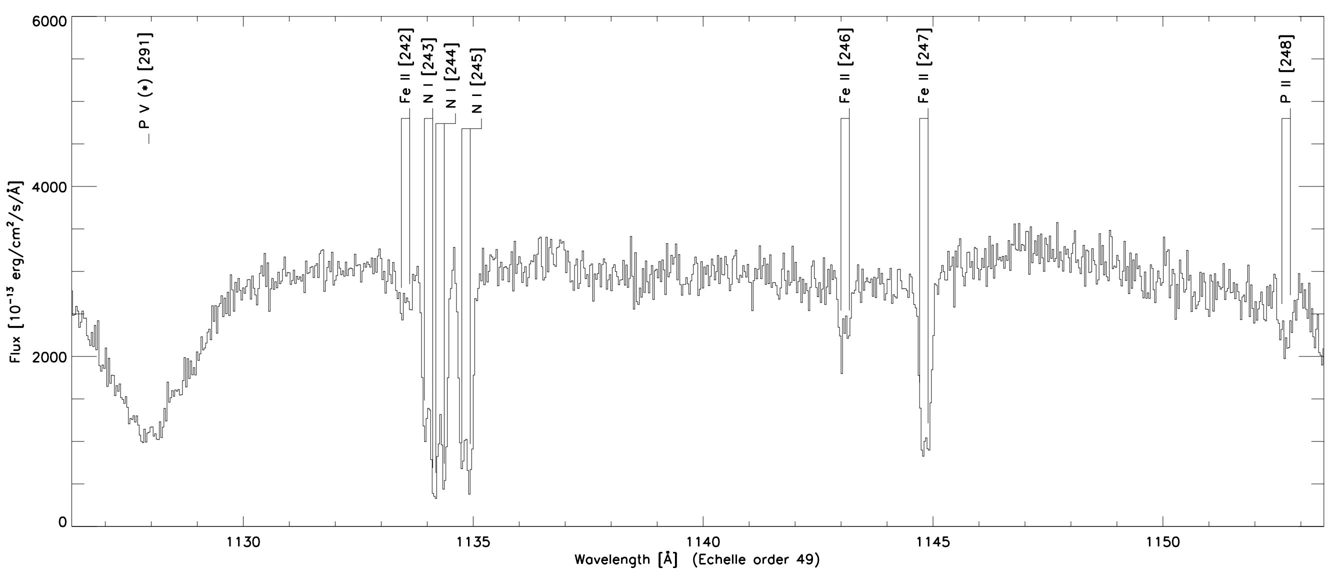
P V (*) [291]
Fe II [242]
N I [243]
N I [244]
N I [245]
Fe II [246]
Fe II [247]
P II [248]
Flux [10⁻¹³ erg/cm²/s/Å]
Wavelength [Å] (Echelle order 49)

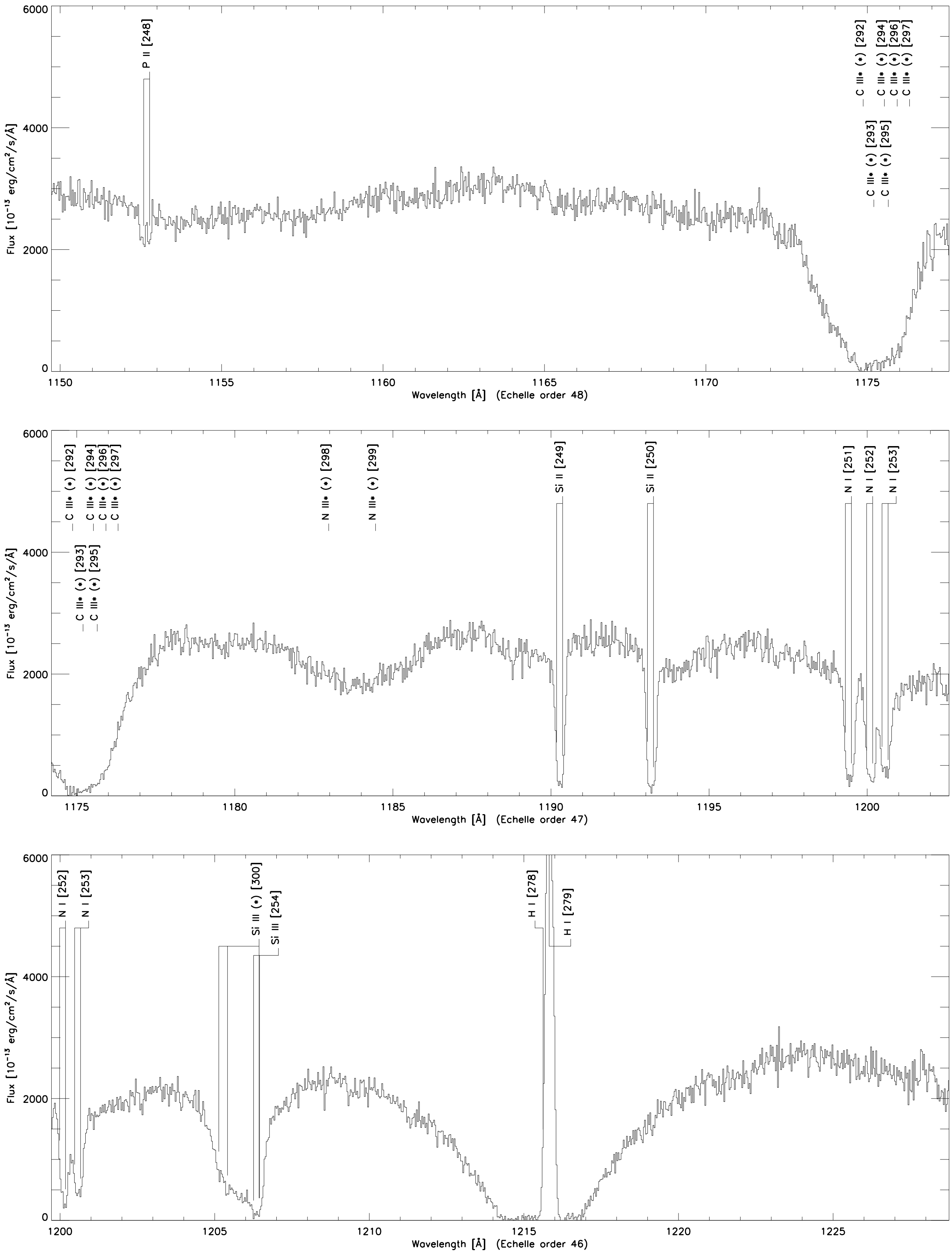
Flux [10⁻¹³ erg/cm²/s/Å]
Wavelength [Å] (Echelle order 48)
P II [248]
C III* (*) [292]
C III* (*) [293]
C III* (*) [294]
C III* (*) [295]
C III* (*) [296]
C III* (*) [297]
Wavelength [Å] (Echelle order 47)
N III* (*) [298]
N III* (*) [299]
Si II [249]
Si II [250]
N I [251]
N I [252]
N I [253]
Wavelength [Å] (Echelle order 46)
Si III (*) [300]
Si III [254]
H I [278]
H I [279]

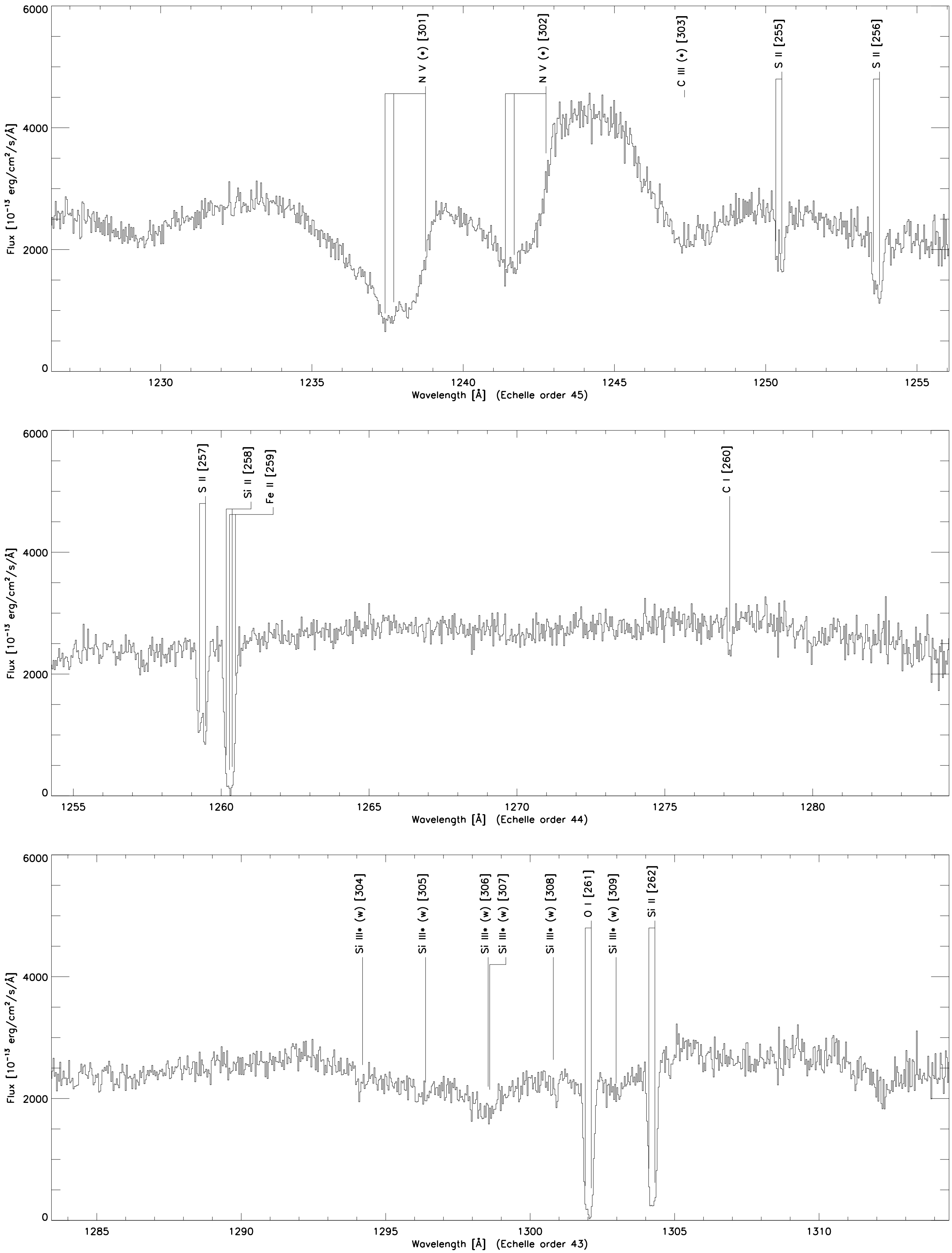
N V (•) [301]
N V (•) [302]
C III (•) [303]
S II [255]
S II [256]
Flux [10⁻¹³ erg/cm²/s/Å]
Wavelength [Å] (Echelle order 45)
S II [257]
Si II [258]
Fe II [259]
C I [260]
Wavelength [Å] (Echelle order 44)
Si III• (w) [304]
Si III• (w) [305]
Si III• (w) [306]
Si III• (w) [307]
Si III• (w) [308]
O I [261]
Si III• (w) [309]
Si II [262]
Wavelength [Å] (Echelle order 43)

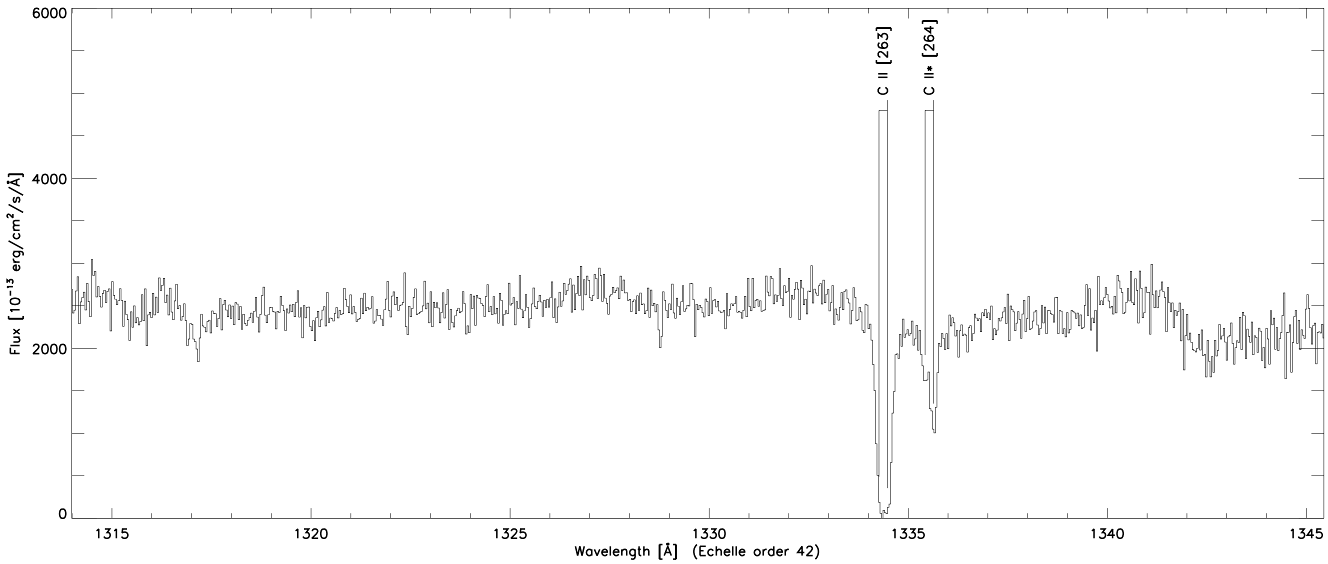
C II [263]
C II* [264]
Flux [10⁻¹³ erg/cm²/s/Å]
0
2000
4000
6000
1315
1320
1325
1330
1335
1340
1345
Wavelength [Å] (Echelle order 42)

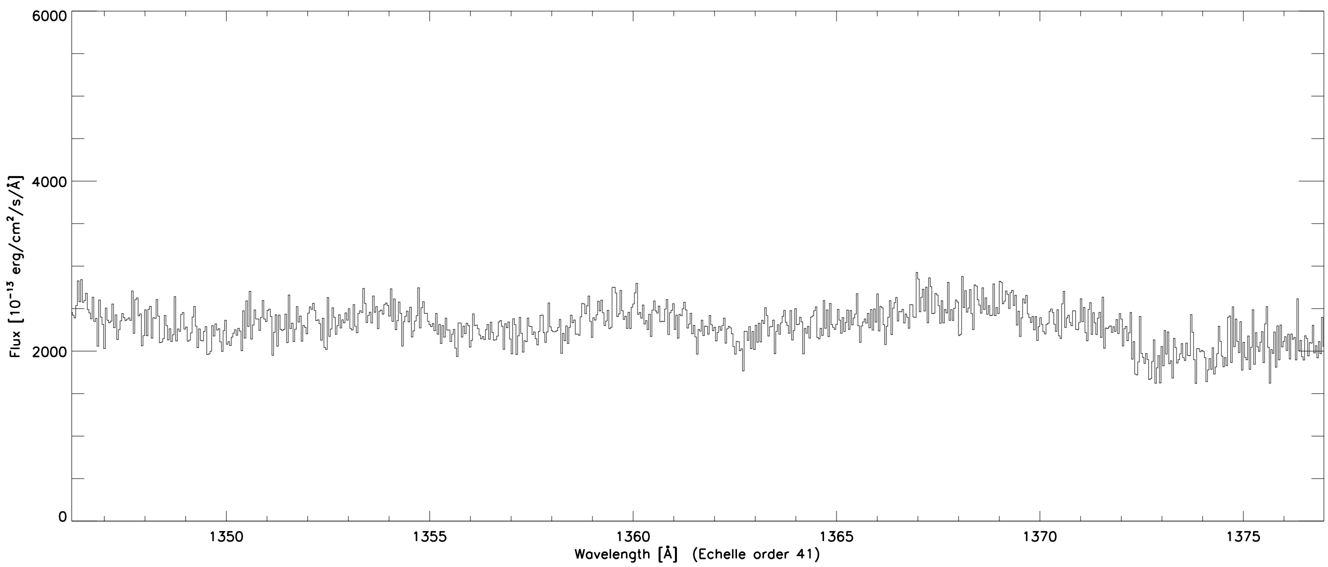
Flux [10⁻¹³ erg/cm²/s/Å]
0
2000
4000
6000
1350
1355
1360
1365
1370
1375
Wavelength [Å] (Echelle order 41)

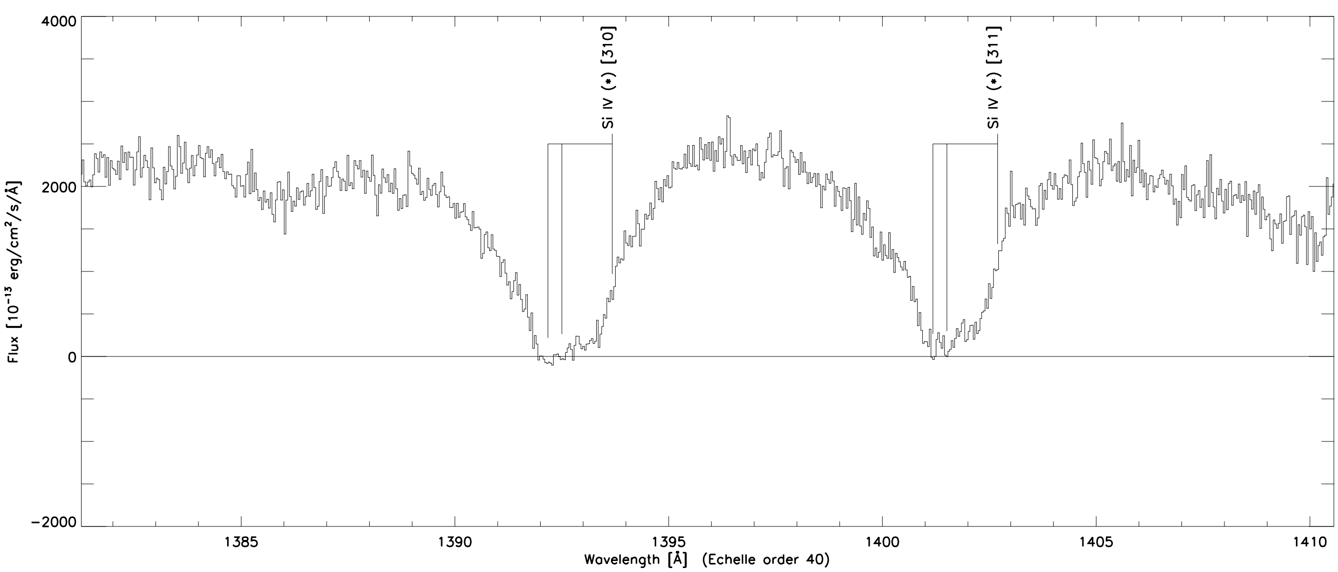
Si IV (*) [310]
Si IV (*) [311]
Flux [10⁻¹³ erg/cm²/s/Å]
−2000
0
2000
4000
1385
1390
1395
1400
1405
1410
Wavelength [Å] (Echelle order 40)